A Soft Switching Bidirectional DC-DC Converter based on Three-State Switching Cell to Photovoltaic Systems Applications

Luan C. S. Mazza, Demercil S. Oliveira Jr., Fernando L. M. Antunes, Diego B. S. Alves,
Paulo C. M. Campelo and Fábio J. L. Freire
FEDERAL UNIVERSITY OF CEARÁ
Centro de Tecnologia - Campus do Pici, Bl. 705
Fortaleza-CE, Brazil
Tel.: +55 / (85) – 3366-9581.
Fax: +55 / (85) – 3366-9574.
E-mail: luanmazza@ifce.edu.br;demercil@dee.ufc.br;fantunes@dee.ufc.br
URL: http://www.dee.ufc.br

Acknowledgements

Keywords

«Bidirectional», «DC-DC Converter», «Photovoltaic», «ZVS».

Abstract

This paper presents a new three-port soft switching dc-dc converter topology based on the bidirectional version of the three-state switching cell, feasible to interconnect battery banks with a dc link and photovoltaic panels. All active switches are designed to operate in Zero Voltage Switching (ZVS). The theoretical analysis and experimental results a 2 kW prototype are presented.

Introduction

Bidirectional dc-dc conversion in photovoltaic systems has been extensively studied and is currently in full development. Several applications require step up from low dc voltage levels (12 V to 48 V) to higher dc voltages (200 V, 311 V or 400 V). Several topologies [1]-[2]-[3] have been developed in recent years for photovoltaic systems. In such applications, the main requirements are high voltage gain, high power density, and high efficiency. Besides, in order to avoid the circulation of leakage currents through the parasitic capacitances, isolation is an interesting solution [4].

The proposed converter is based on the bidirectional dc-dc Dual Active Bridge (DAB) converter, which is very attractive because of its features including ZVS, bidirectional power flow, low stress regarding the involved components, and high power density [5], [6]. Moreover, the DAB is widely applied in dc distribution systems, UPSs (Uninterruptible Power Supplies), bidirectional power flow dc systems [7], [8], [9] and ac-dc power systems [10].

Considering that most usual electronic loads e.g. TV, personal computers, audio systems, electronic ballasts, and many others can be directly connected to a 311-V dc link, an architecture for a dc distribution system is shown in Fig. 1. Each photovoltaic module is connected to the 311-V dc link through individual dc-dc converters that perform MPPT (Maximum Power Point Tracking). Electronic loads are connected to the dc link and a dc-ac bidirectional converter is responsible for interconnecting the system to the ac mains.

The proposed converter is used to interconnect the 311-V dc link to the battery bank, with consequent flexible energy management that characterizes smart grids. Additionally, it is possible to connect photovoltaic panels to the converter, thus avoiding the use of an additional dc-dc stage.
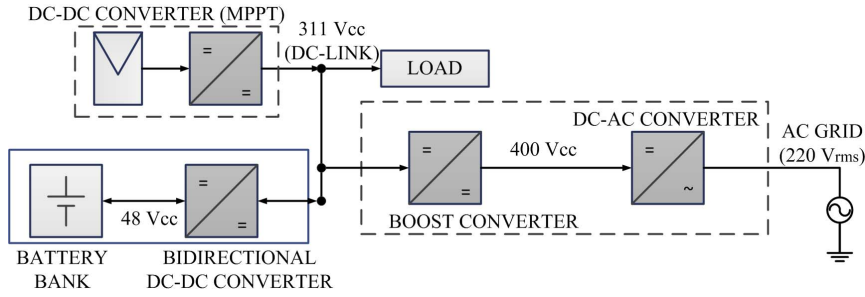
Fig. 1: Proposed photovoltaic system proposed based on DAB-3SSC.

Proposed topology

The proposed converter is based on the DAB [5] and the Three-State Switching Cell (3SSC) [11], as shown in Fig. 2 (a). Various other converters are based on 3SSC [12] and [13]. Besides topologies with high voltage gain [14]-[15]-[16]. And also with characteristics similar to the one presented here [17]-[18]. An initial study of this topology is presented in [19].

(a)   (b)
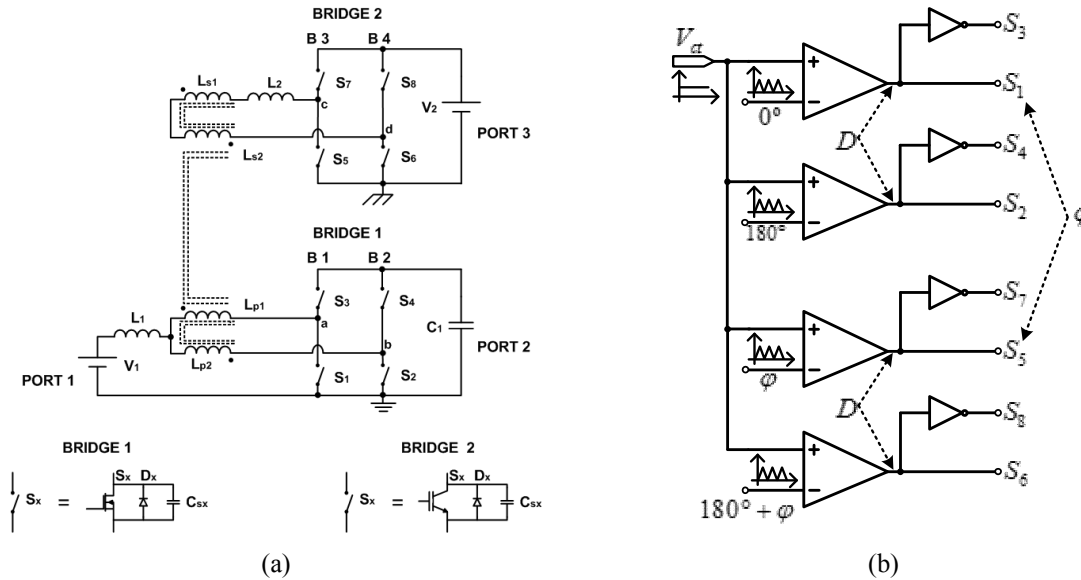
Fig. 2: DAB-3SSC topology: (a) Proposed topology; (b) Modulation strategy.

Principle of operation

The switches are driven as described: the duty cycle (D) is applied to the lower switches at the primary and secondary sides. Additionally, the primary legs are phase-shifted by 180º as well as the secondary ones. Then voltage Vab is applied to the primary side and voltage Vcd is applied to the secondary side. Parameter φ is defined as the phase-shift angle between the fundamental components of voltages V_{ab} and V_{cd}. The modulation strategy of the converter is presented in Fig. 2 (b). Thus, the proposed modulation results in sixteen possible operation regions, as shown in Fig. 3 (a). Fig. 3 (b) presents the main waveforms.

First stage

This stage begins with the switch S_3 for switching the switch S_1. The switches S_2, S_6 and S_7 remain in conduction. The current i_1 on port 1 flowing through the inductor L_1 grows linearly. The currents in the primary one, i_{p1}, and 2 i_{p2}, increase and decrease linearly, respectively. The capacitor is C1 with its zero ic1 current. Already current in the secondary of the transformer i_s decreases linearly until it reaches the maximum negative value. In this step, no power transfer to V_2, as presented in Fig. 4 (a).
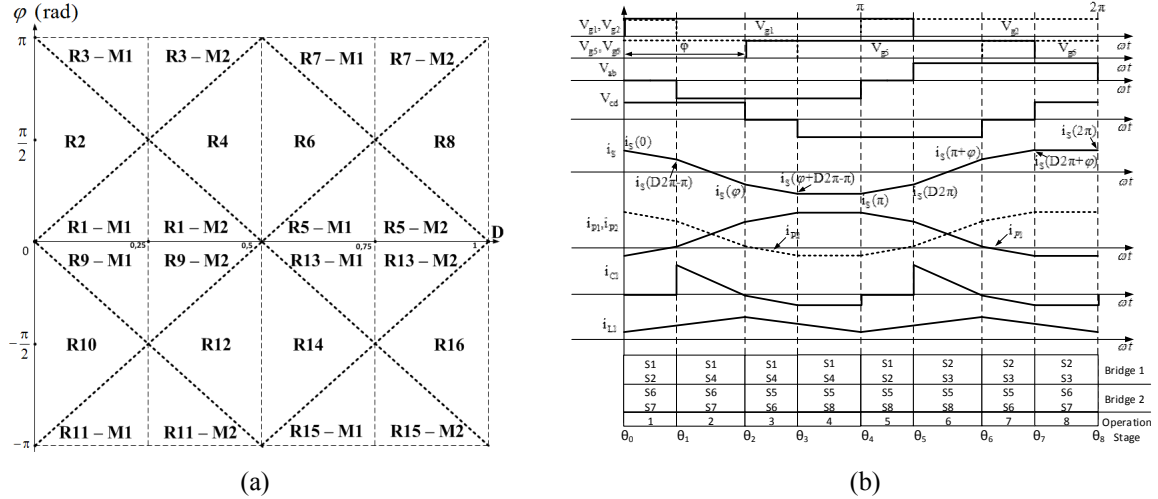
Fig. 3: DAB-3SSC topology: (a) Operation regions; (b) Main waveforms.

Second stage

This stage begins by switching switch S_2 to the switch S_4. The switches S_1, S_6 and S_7 remain in conduction. The current i_1 decreases. The i_{p1} and i_{p2} currents continue increasing and decreasing, respectively. The current I_s remains downward. In this stage, no power transfer to V_2, as presented in Fig. 4 (b).
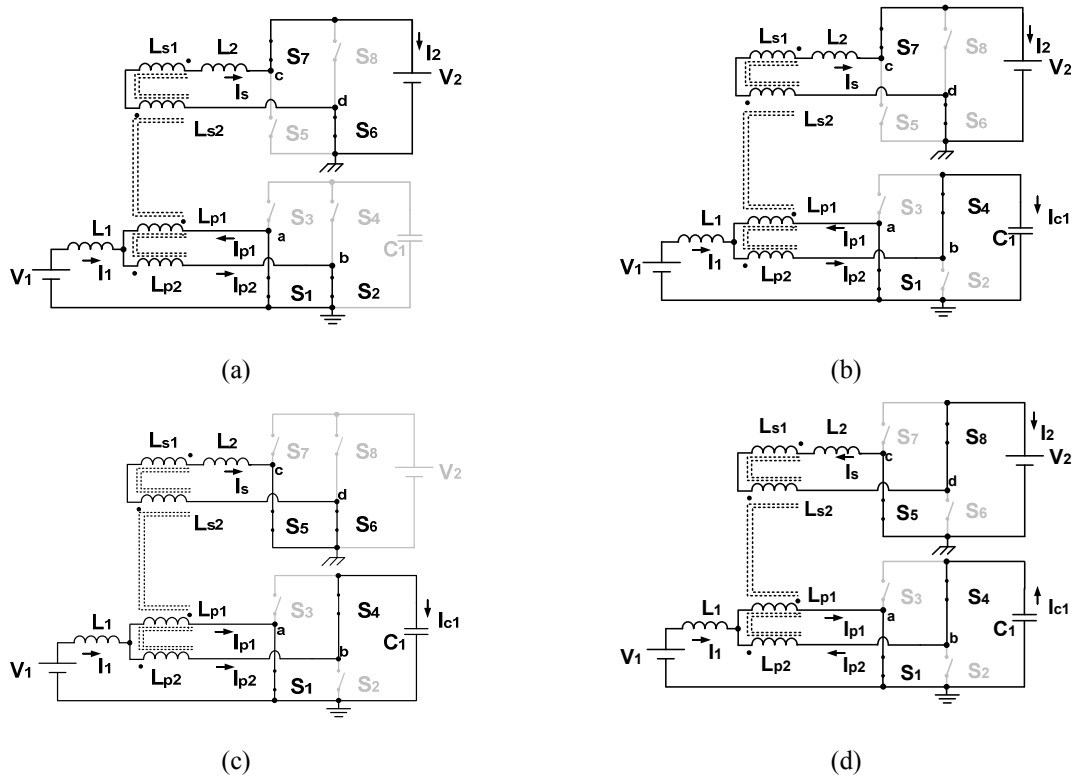

Fig. 4: DAB-3SSC operation stages: (a) First; (b) Second; (a) Third; (b) Fourth.

Third stage

This stage begins with the switching of the S_7 switch to the S_5 switch. The switches S_1, S_4 and S_6 continue to conduct. The current start value i_1 in $I_{1,\,max}$, and decreases linearly, or transferring energy from the inductor to the circuit L_1. The current i_{p1} decreases to zero, while the i_{p2} current increases linearly, and changes direction, to be responsible for all C_1 capacitor charging current at the end of the stage. The chain starts with i_s in $I_{s,max}$ and then grows linearly to reverse direction. In this step, no power transfer to V_2, as shown in Fig. 4 (c).

Fourth stage

This stage begins with the switching of the switch S_6 to S_8 switch. The switches S_1, S_4 and S_5 remain in conduction. The current i_1 continues with decreasing value and thus transferring energy L_1 inductor to the circuit. The current i_{p1} remains at zero value throughout this step, since the current i_{p2} remains constant value, as well as the current i_{C1} the C_1 capacitor. Because of the configuration in the switch, the current i_s remains constant throughout this step. In this step, no power transfer to V_2, as presented in Fig. 4 (d).

Quantitative analysis

In this section, we present the equivalent electrical circuits to each operating step, aiming to perform mathematical analysis. The equivalent circuit is that the secondary for simplicity. Following the equivalent circuits are presented for the first 4 stages of operation and their equations, aiming at further raising the output characteristic curve.

As the converter has sixteen operating regions, this section is shown only to R6 region. But in the end presents the static gain of all regions.
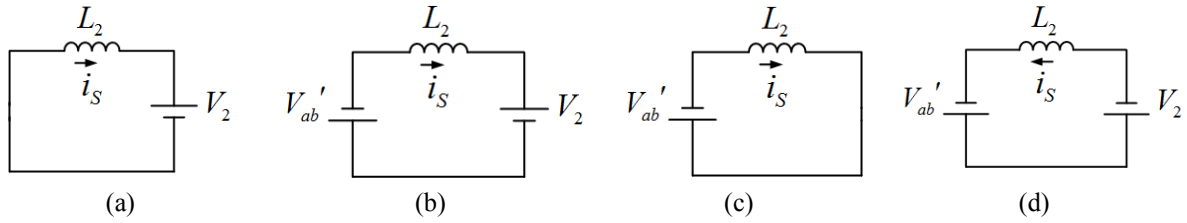

Fig. 5: DAB-3SSC stage equivalent circuit: (a) First; (b) Second; (c) Third; (d) Fourth.

First Stage

Fig. 5 (a) presents the equivalent circuit of the first converter operation step operating in region R6.

Analyzing Fig. 5 (a), may be deduced from the equations (1) and (2).

$$V_{L_2} = -V_2 \tag{1}$$

$$i_{S(I)}(\theta) = \left(\frac{-V_2}{\omega L_2}\right)\theta + i_S(0) \tag{2}$$

The final angle of this operation phase is defined by equation (3).

$$\theta_1 = (2D-1)\pi \tag{3}$$

Substituting angular value (3) of the stage in equation (2), we obtain expression (4).

$$i_S([2D-1]\pi) = -\left(\frac{V_2}{\omega L_2}\right)([2D-1]\pi) + i_S(0) \tag{4}$$

Second stage

Fig. 5 (b) presents the equivalent circuit of the first converter operation step operating in region R6.

Analyzing Fig. 5 (b), may be deduced from the equations (5) and (6).

$$V_{L_2} = -V_{ab}' - V_2 \tag{5}$$

$$i_{S(II)}(\theta) = \left(\frac{-V_{ab}' - V_2}{\omega L_2}\right)(\theta - [2D-1]\pi) + i_S([2D-1]\pi) \tag{6}$$

The final angle of this operation phase is defined by equation (7).

$$\theta_2 = \varphi \tag{7}$$

Substituting angular value (7) of the stage in equation (6), we obtain expression (8).

$$i_S(\varphi) = \left(\frac{-V_{ab}' - V_2}{\omega L_2}\right)(\varphi - [2D-1]\pi) + i_S([2D-1]\pi) \tag{8}$$

Third stage

Fig. 5 (c) presents the equivalent circuit of the first converter operation step operating in region R6. Analyzing Fig. 5 (c) may be deducted from the equations (9) and (10).

$$V_{L_2} = -V_{ab}' \tag{9}$$

$$i_{S(III)}(\theta) = \left(\frac{-V_{ab}'}{\omega L_2}\right)(\theta - \varphi) + i_S(\varphi) \tag{10}$$

The final angle of this operation phase is defined by equation (11).

$$\theta_3 = \varphi + (2D-1)\pi \tag{11}$$

Substituting angular value (11) of the stage in equation (10), we obtain expression (12).

$$i_S(\varphi + [2D-1]\pi) = \left(\frac{-V_{ab}'}{\omega L_2}\right)([2D-1]\pi) + +i_S(\varphi) \tag{12}$$

Fourth stage

Fig. 5 (d) presents the equivalent circuit of the first converter operation step operating in region R6. Analyzing Fig. 5 (d), may be deducted from the equations (13) and (14).

$$V_{L_2} = -V_{ab}' + V_2 \tag{13}$$

$$i_{S(IV)}(\theta) = \left(\frac{-V_{ab}' + V_2}{\omega L_2}\right)(\theta - \varphi - (2D-1)\pi) + i_S(\varphi + (2D-1)\pi) \tag{14}$$

The final angle of this operation phase is defined by equation (15).

$$\theta_4 = \pi \tag{15}$$

Substituting angular value (15) of the stage in equation (14), we obtain expression (16).

$$i_S(\pi) = \left(\frac{-V_{ab}' + V_2}{\omega L_2}\right)(2\pi - \varphi - D2\pi) + i_S(\varphi + (2D-1)\pi) \tag{16}$$

The average value of the output current in port 3 (I2) is calculated using equation (17). For the power transfer to the output of gate occurs in stage 1, 3 and 4.

$$I_2 = \frac{2}{\omega T_s}\left[\underbrace{\int_0^{(2D-1)\pi} i_{S(I)}(\theta)d\theta}_{Expressão\ 1} + \underbrace{\int_{(2D-1)\pi}^{\varphi} i_{S(II)}(\theta)d\theta}_{Expressão\ 2} - \underbrace{\int_{\varphi+(2D-1)\pi}^{\pi} i_{S(IV)}(\theta)d\theta}_{Expressão\ 3}\right] \quad (17)$$

Because the AC current in the secondary is symmetrical, it can be observed that:

$$\begin{cases} i_S(0) = -i_S(\pi) \\ i_S([2D-1]\pi) = -i_S(D2\pi) \\ i_S(\varphi) = -i_S(\pi+\varphi) \\ i_S(\varphi+[2D-1]\pi) = -i_S(\varphi+D2\pi) \end{cases} \quad (18)$$

Applying the conditions of (18) in equations (4), (8), (12) and (16) and solving to $i_S(0)$ $i_S([2D-1]\pi)$ and $i_S(\varphi+[2D-1]\pi)$ to find the initial current in the stages 1, 3 and 4, is obtained the equations (19) (20) and (21).

$$i_S(0) = \frac{V_{ab}'\pi - V_{ab}'D\pi - V_2\pi + V_2\varphi + V_2D\pi}{\omega L_2} \quad (19)$$

$$i_S([2D-1]\pi) = \frac{V_{ab}'\pi - V_{ab}'D\pi + V_2\varphi - V_2D\pi}{\omega L_2} \quad (20)$$

$$i_S(\varphi+[2D-1]\pi) = \frac{1}{\omega L_2}\begin{pmatrix} V_{ab}'\pi - V_{ab}'\varphi - V_{ab}'D\pi - \\ V_2\pi + V_2D\pi \end{pmatrix} \quad (21)$$

Making explicit the expressions 1, 2 and 3 of equation (17) and substituting it equations (19) (20) and (21), is obtained equations (22) (23) and (24).

$$\int_0^{(2D-1)\pi}\left(\frac{-V_2}{\omega L_2}\right)\theta d\theta + \int_0^{(2D-1)\pi}\left(\frac{V_{ab}'\pi - V_{ab}'D\pi - V_2\pi + V_2\varphi + V_2D\pi}{\omega L_2}\right)d\theta \quad (22)$$

$$\int_{(2D-1)\pi}^{\varphi}\left(\frac{-V_{ab}'-V_2}{\omega L_2}\right)(\theta-[2D-1]\pi)d\theta + \int_{(2D-1)\pi}^{\varphi}\left(\frac{V_{ab}'\pi - V_{ab}'D\pi + V_2\varphi - V_2D\pi}{\omega L_2}\right)d\theta \quad (23)$$

$$\int_{\varphi+(2D-1)\pi}^{\pi}\left(\frac{-V_{ab}'+V_2}{\omega L_2}\right)(\theta-\varphi-(2D-1)\pi)d\theta + \int_{\varphi+(2D-1)\pi}^{\pi}\left(\frac{1}{\omega L_2}\right)\begin{pmatrix} V_{ab}'\pi - V_{ab}'\varphi - V_{ab}'D\pi \\ -V_2\pi + V_2D\pi \end{pmatrix}d\theta \quad (24)$$

Solving equations (22), (23) and (24), and substituting in equation (17), we obtain the average current in the output port 3 (25).

$$I_2 = \frac{V_{ab}'}{\omega L_2}\left(-\frac{\varphi^2}{\pi} + \varphi + D2\pi - D^2 2\pi - \frac{\pi}{2}\right) \quad (25)$$

Since Vab' is given by (26):

$$V_{ab}' = \frac{V_1 a}{(1-D)} \tag{26}$$

Calculating the ratio between the average current of the output port 3 to the converter input voltage V1 port 1, this gives the static gain region R6 (27).

$$G_{R6} = \frac{I_2}{V_1} = \frac{a}{(1-D)\omega L_2}\left(-\frac{\varphi^2}{\pi} + \varphi + D2\pi - D^2 2\pi - \frac{\pi}{2}\right) \tag{27}$$

Realizing the same procedure for the other regions, obtains the static gain as a function of phase shift (φ). The Table I and Fig. 7 (a) presented the static gain of the converter for all operating regions.

Table I. Power in port 3.

Region (R)	Power in port 3 (p.u.) - P_2	
	$\varphi \geq 0$	$\varphi < 0$
R1/R9	$d\left(-\dfrac{\varphi^2}{2\pi} + D2\varphi\right)$	$d\left(\dfrac{\|\varphi\|^2}{2\pi} - D2\|\varphi\|\right)$
R2/R10	$d\left(D^2 2\pi\right)$	$-d\left(D^2 2\pi\right)$
R3/R11	$d\left(-\dfrac{\varphi^2}{2\pi} + \varphi - D2\varphi + D2\pi - \dfrac{\pi}{2}\right)$	$d\left(\dfrac{\|\varphi\|^2}{2\pi} - \|\varphi\| + D2\|\varphi\| - D2\pi + \dfrac{\pi}{2}\right)$
R4/R12	$d\left(-\dfrac{\varphi^2}{\pi} + \varphi + D2\pi - D^2 2\pi - \dfrac{\pi}{2}\right)$	$d\left(\dfrac{\|\varphi\|^2}{\pi} - \|\varphi\| - D2\pi + D^2 2\pi + \dfrac{\pi}{2}\right)$
R5/13	$d\left(-\dfrac{\varphi^2}{2\pi} + 2\varphi - D2\varphi\right)$	$d\left(\dfrac{\|\varphi\|^2}{2\pi} - 2\|\varphi\| + D2\|\varphi\|\right)$
R6/R14	$d\left(-\dfrac{\varphi^2}{\pi} + \varphi + D2\pi - D^2 2\pi - \dfrac{\pi}{2}\right)$	$d\left(\dfrac{\|\varphi\|^2}{\pi} - \|\varphi\| - D2\pi + D^2 2\pi + \dfrac{\pi}{2}\right)$
R7/R15	$d\left(\dfrac{-\varphi^2}{2\pi} - \varphi + D2\varphi - D2\pi + \dfrac{3\pi}{2}\right)$	$d\left(\dfrac{\|\varphi\|^2}{2\pi} + \|\varphi\| - D2\|\varphi\| + D2\pi - \dfrac{3\pi}{2}\right)$
R8/R16	$d\left(D^2 2\pi - D4\pi + 2\pi\right)$	$-d\left(D^2 2\pi - D4\pi + 2\pi\right)$

Soft switching analysis

The analysis of soft switching conditions for all regions leads to the curve in Fig. 7 (b) considering D=0.5 and d=1 (relationship between V_{cd} and V_{ab} reflected secondary). It can be noticed that the converter operates with soft switching characteristic for all switches. Any variation around the aforementioned conditions narrows the soft switching regions.

Experimental Results

The prototype was developed for a nominal power of 2 kW, utilizing the port 1 to voltage 48 V and port 3 is a 311 V voltage. Fig. 8 presented a photograph of the implemented prototype. The Table II shown prototype specifications
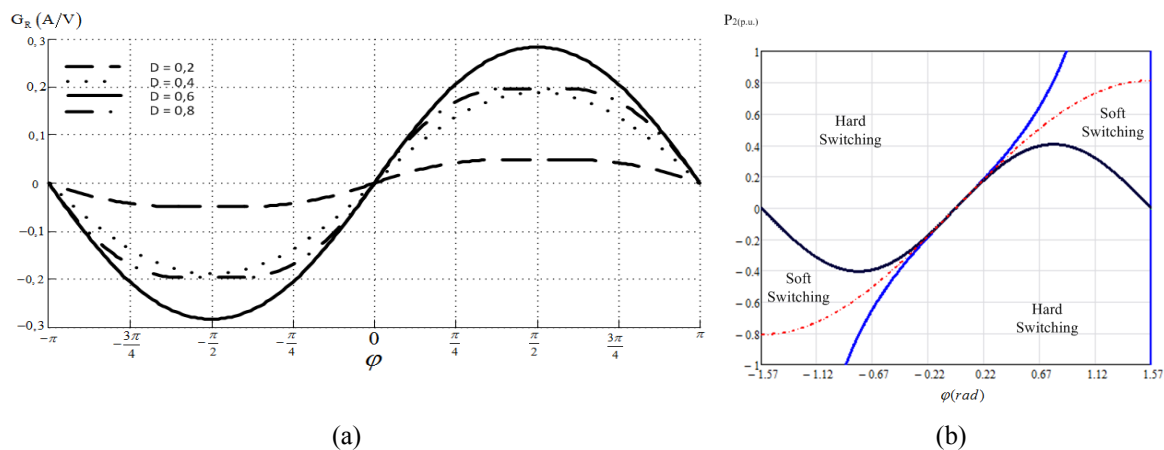
Fig. 7: DAB-3SSC topology: (a) Static gain in function of φ and D as parameter; (b) Soft switching regions.

Table II. Prototype specifications.

Switching frequency (f_s)	50 kHz
Port 1 voltage (V_1)	48 V
Port 3 voltage (V_2)	311 V
Load power (P_2)	2 kW
Input inductance (L_1)	42 uH
Leakage inductance (L_2)	65 uH
Capacitor (C_1)	203 uF
Output capacitor (C_2)	230 uF
Transformer relationship (a)	1:3,2

The experimental results are divided into: Mode Charge Battery Bank (MCBB) and Mode Discharge Battery Bank (MDBB).

Mode Discharge Battery Bank (MDBB)

The experimental results are presented in Fig. 9 to MDBB. The input inductor current IL1, the output current without filtering, primary currents i_{p1} and i_{p2}, voltages V_{ab} and V_{cd} (where phase-shift can be clearly noticed), and also the current through inductor L_2 are the represented waveforms.
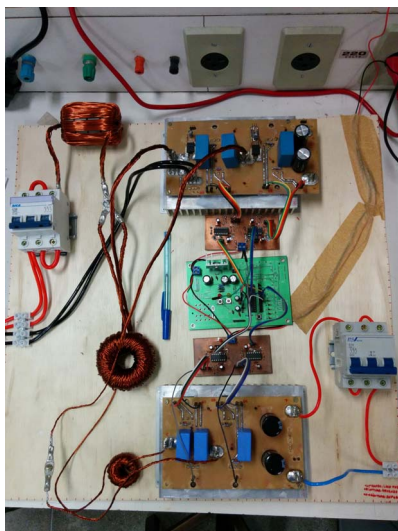

Fig. 8: Photography experimental prototype.

The Fig. 9 (a) and 9 (b) shows the soft switching in the switches S_1 and S_5. The efficiency curve is shown in Fig. 11 (a). The maximum yield is obtained at the value P_2 at approximately 680 W in MDBB.
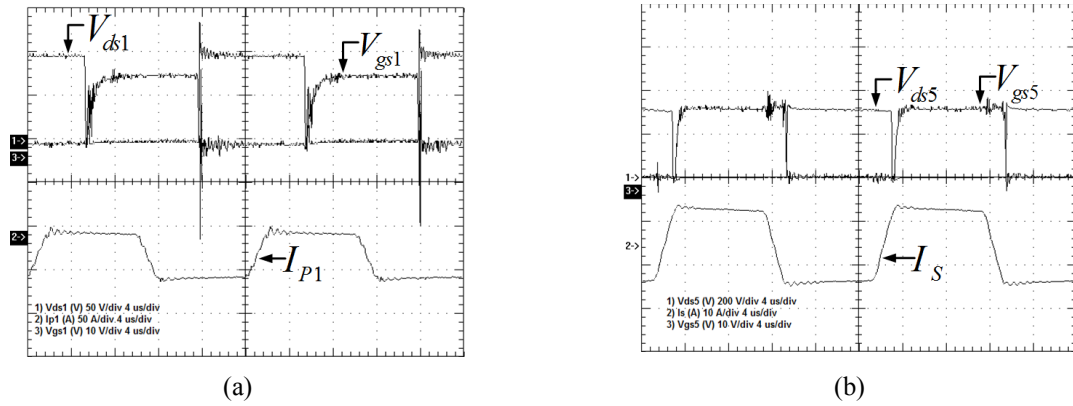
Fig. 9: Experimental results for D=0.51 and φ=π/6 in MDBB: (a) Drain source and gate source voltage in S_1 and primary 1 current; (b) Drain source and gate source voltage in S_5 and secondary current.

Mode Discharge Battery Bank (MCBB)

The experimental results are presented in Fig. 10 to MCBB. The Fig. 10 (a) and 10 (b) shows the soft switching in the switches S_1 and S_5. The efficiency curve is shown in Fig. 11 (b). The maximum yield is obtained at the value P_1 at approximately 900 W in MCBB.
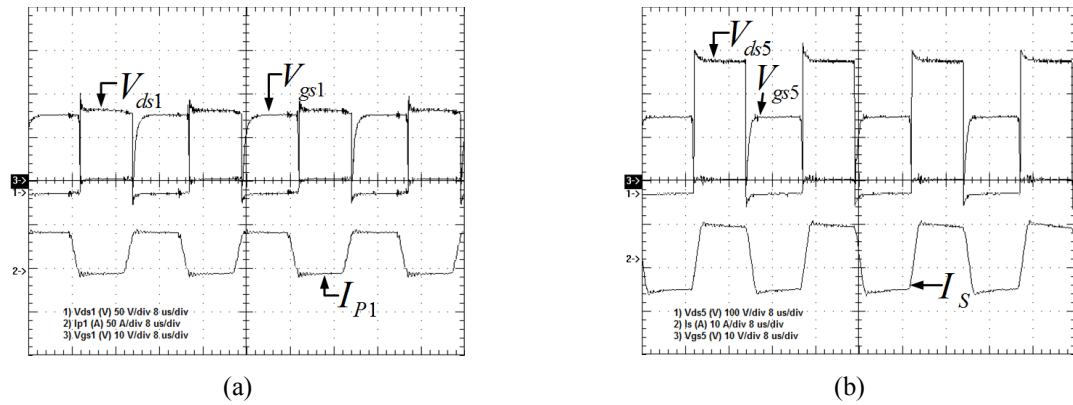

Fig. 10: Experimental results for D=0.51 and φ=π/6 in MCBB: (a) Drain source and gate source voltage in S_1 and primary 1 current; (b) Drain source and gate source voltage in S_5 and secondary current.
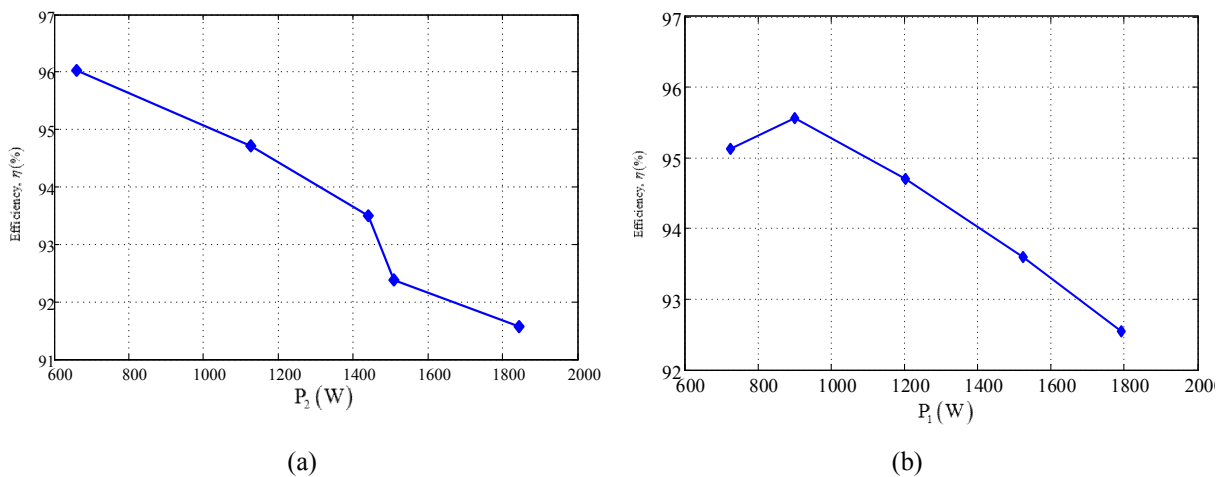

Fig. 11: DAB-3SSC experimental results: (a) Efficiency curve in MDBB; (b) Efficiency curve in MCBB.

Conclusion

This paper has proposed a bidirectional converter based on the DAB-3SSC. The main advantage of the topology is the high frequency isolation and ZVS operation for all switches over a wide load range, what implies high efficiency. Also, bidirectional power flow, and three-port characteristic are remarkable advantages of the proposed converter. Although this study focuses on photovoltaic systems with battery banks, it presents a promising converter for applications in other approaches.

References

[1] L. H. S. C. Barreto, P. P. Praça, D. S. Oliveira, R. N. A. L Silva, "High Voltage Gain Boost Converter Based on Three-State Commutation Cell for Battery Charging Using PV Panels in a Single Conversion Stage", IEEE Trans. Power Electron., Vol. 29, n. 1, pp. 150-158, Jan. 2014.

[2] R. J. Wai, R. Y. Duan, "High-efficiency DC/DC converter with high voltage gain" Electric Power Applications, IEE Proceedings, vol.152, no.4, pp. 793- 802, Jul. 2005.

[3] Y. M. Chen, A. Q. Huang, X. Yu, (2013). "A High Step-Up Three-Port DC-DC Converter for Stand-Alone PV/Battery Power Systems", IEEE Trans. Power Electron., Vol. 28, No 11, November 2013.

[4] R. Teodorescu, M. Liserre and P. Rodríguez, Grid Converters for Photovoltaic and Wind Power Systems, PPiscataway, Nj: IEEE Wiley Interscience, 2011.

[5] R. W. De Doncker, D. M. Divan, M. H. Kheraluwala, "A three-phase soft-switched high power density DC/DC converter for high power applications", IEEE Trans. on Industry Applications, Vol. 27, n. 1, pp. 63-73, Jan/Feb. 1991.

[6] M. H. Kheraluwala, R. W. Gascoigne, D. M. Divan, E. D. Baumann, "Performance characterization of a high-power dual active bridge dc-todc converter", IEEE Trans. Power Electron., vol. 28, n. 6, pp. 1294–1301, Nov.-Dec. 1992.

[7] J. Kim, I. Jeong, K. Nam, "Asymmetric duty control of the dual-active-bridge DC/DC converter for single-phase distributed generators", in ECCE - IEEE Energy Conversion Congress and Exposition, 2009, pp. 85-72.

[8] J. L. Duarte, M. Hendrix, M. G. Simoes, "Three-port bidirectional converter for hybrid fuel cell systems", IEEE Trans. Power Electron., vol. 22, n. 2, pp. 480–487, Mar. 2007.

[9] C. M. Hong, L. S. Yang, T. J. Liang, J. F. Chen, "Novel Bidirectional DC-DC Converter with High Step-Up/Down Voltage Gain. Energy Conversion," Congress and Exposition, 2009. ECCE 2009. pp.60-66.

[10] Z. Qian, O. A. Rahman, H. Hu, I. Batarseh, "An Integrated Three-Port Inverter for Stand-Alone PV Applications," In Proc. IEEE Energy Conversion Congress & Expo, Atlanta, USA, 2010.

[11] H. M. Tao, A. Kotsopoulos, J. L. Duarte, M. A. M. Hendrix, "Transformer-coupled multiport ZVS bidirectional dc-dc converter with wide input range", IEEE Trans. Power Electron., vol. 23, n. 2, pp. 771–781, Mar. 2008.

[12] G. V. Torrico Bascopé and I. Barbi, "Generation of a Family of Non-Isolated DC-DC PWM Converters Using New Three-State Switching Cells", in IEEE Power Eletronic Specialists Conference, 2000, pp. 858-863.

[13] Y. J. A. Alcazar, D. S. Oliveira Jr., F. L. Tofoli, R. P. Torrico-Bascopé, "DC-DC Nonisolated Boost Converter Based on The Three-State Switching Cell and Voltage Multiplier Cells," IEEE Transactions on Industrial Electronics, vol. 60, no. 10, pp. 4438–4449, Oct. 2013.

[14] P. P. Praça, G. A. L. Henn, D. S. Oliveira, L. H. S. C. Barreto, R. N. A. L Silva, "High Voltage Gain Single Stage DC-DC Converter Based on Three-State Commutation Cell," Applied Power Electronics Conference and Exposition (APEC), pp. 2882-2887, March 2013.

[15] L. H. S. C. Barreto, P. P. Praça, G. A. L. Henn, R. N. A. L. Silva, D. S. Oliveira, "High Voltage Gain Boost Converter Battery Charger Applied to PV Systems," IEEE Trans. Power Electron., pp. 1526-1531, 2011.

[16] G. V. T. Bascopé, R. P. T. Bascopé, D. S. Oliveira Jr., F. L. M. Antunes, C. G. C. Branco, "A High Step-Up Dc-Dc Converter Based on Three-State Switching Cell," in Industrial Electronics, IEEE International Symposium, 2006, Vol. 2, pp 998-1003.

[17] P. P. Praça, G. A. L. Henn, R. N. A. L. Silva, D. S. Oliveira, L. H. S. C. Barreto,"A Single Stage High Voltage Gain ZVS Boost Converter Feasible to Photovoltaic Battery Charger Systems," In IX International Conference on Industry Applications (INDUSCON), 2010, São Paulo – SP.

[18] D. B. S. Alves, P. P. Praça, D. S. Oliveira, L. H. S. C. Barreto, "A Single Stage High Voltage Gain Boost Converter Based on the Three-State Switching Cell," In PCIM South America, São Paulo-SP, Brazil, 2014.

[19] Luan C. S. Mazza, D. S. Oliveira, Fernando L. M. Antunes, Diego B. S. Alves, Paulo C. M. Campelo, Fábio J. L. Freire "A Soft Switching Bidirectional DC-DC Converter with High Frequency Isolation Feasible to Photovoltaic System Applications", In PCIM Europe, Nuremberg, Germany, 2015.